

## GATraj: A graph- and attention-based multi-agent trajectory prediction model

Hao Cheng <sup>a,\*<sup>1</sup></sup>, Mengmeng Liu <sup>a,1</sup>, Lin Chen <sup>c</sup>, Hellward Broszio <sup>c</sup>, Monika Sester <sup>b</sup>, Michael Ying Yang <sup>a,\*</sup>

<sup>a</sup> Faculty of Geo-Information Science and Earth Observation (ITC), University of Twente, Netherlands

<sup>b</sup> Institute of Cartography and Geoinformatics, Leibniz University Hannover, Germany

<sup>c</sup> VISCODA GmbH, Germany



### ARTICLE INFO

#### Keywords:

Trajectory prediction  
Graph model  
Autonomous driving  
Pedestrian  
Mixture density network

### ABSTRACT

Trajectory prediction has been a long-standing problem in intelligent systems like autonomous driving and robot navigation. Models trained on large-scale benchmarks have made significant progress in improving prediction accuracy. However, the importance on efficiency for real-time applications has been less emphasized. This paper proposes an attention-based graph model, named *GATraj*, which achieves a good balance of prediction accuracy and inference speed. We use attention mechanisms to model the spatial-temporal dynamics of agents, such as pedestrians or vehicles, and a graph convolutional network to model their interactions. Additionally, a Laplacian mixture decoder is implemented to mitigate mode collapse and generate diverse multimodal predictions for each agent. *GATraj* achieves state-of-the-art prediction performance at a much higher speed when tested on the ETH/UCY datasets for pedestrian trajectories, and good performance at about 100 Hz inference speed when tested on the nuScenes dataset for autonomous driving. We conduct extensive experiments to analyze the probability estimation of the Laplacian mixture decoder and compare it with a Gaussian mixture decoder for predicting different multimodalities. Furthermore, comprehensive ablation studies demonstrate the effectiveness of each proposed module in *GATraj*.

### 1. Introduction

Accurately predicting the movements of agents, such as pedestrians and vehicles, in various environments is crucial for many intelligent systems, including autonomous driving and robot navigation. One application is that, with accurate predictions of other agents' trajectories in the vicinity, an automated ego agent can safely navigate its own path. However, predicting trajectories is challenging for several reasons. First, agents' behaviors are stochastic, as they mutually influence each other, for instance, by avoiding collisions or staying closely in a subgroup. Second, the information available to derive an agent's behavior is often limited, and their destination is typically unknown. In most cases, the ego agent can only estimate other agents' behaviors based on their perceived past moving dynamics, such as velocity and heading direction, and interactions depending on their relative positions with their environments. Moreover, due to the mutual influence among agents and their movements in both spatial and temporal dimensions, an agent's behavior can be multimodal in terms of moving into different directions at various speeds. Therefore, trajectory prediction needs

to consider both spatial-temporal dynamics and the multimodality of agents' behaviors.

The accuracy of trajectory prediction across multiple benchmarks has been significantly enhanced by recent deep learning models trained on large-scale real-world datasets, as demonstrated in Fig. 1 by the y-axis representing the displacement errors measured by Euclidean distance. These models accomplish the prediction task by utilizing one or more of the following sources of information:

**Observations of the past trajectories.** The input for trajectory prediction tasks includes an agent's past trajectory in both lateral and longitudinal coordinates, as well as the trajectories of its neighboring agents observed in the vicinity. In pedestrian trajectory prediction tasks on the ETH/UCY benchmark (Pellegrini et al., 2009; Lerner et al., 2007), a popular time horizon setting is for the model to observe eight time steps and predict the next 12 time steps at a sampling rate of 2.5 Hz. For autonomous driving on the nuScenes benchmark (Caesar et al., 2020), the model typically observes up to four time steps and predicts the next 12 time steps at a sampling rate of 2 Hz. More recent datasets, such as those introduced in Chang et al. (2019), Sun et al.

\* Corresponding authors.

E-mail addresses: [h.cheng-2@utwente.nl](mailto:h.cheng-2@utwente.nl) (H. Cheng), [michael.yang@utwente.nl](mailto:michael.yang@utwente.nl) (M.Y. Yang).

<sup>1</sup> Equal contribution.

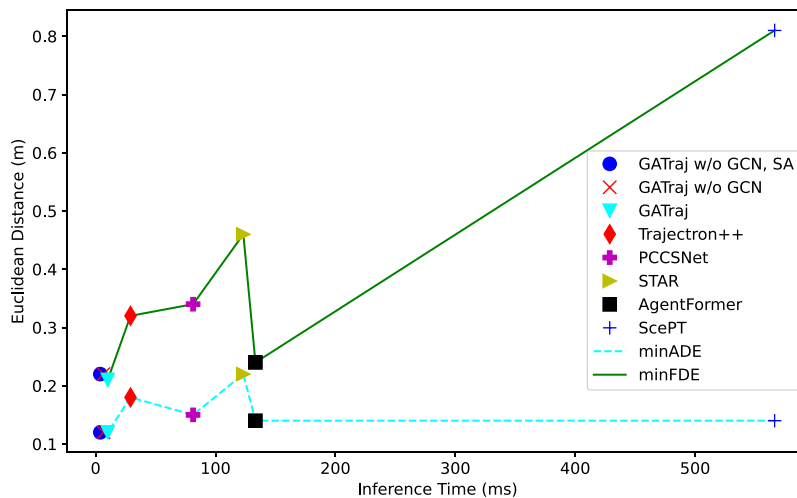


**Fig. 1.** The inference speed and the prediction performance of the models on the Zara2 dataset (Lerner et al., 2007) computed from a single Tesla V100 GPU. GATraj runs faster than other prediction methods and achieves superior performance. SA: self-attention (Vaswani et al., 2017); GCN: graph convolutional network (Welling and Kipf, 2017).

(2020) and Wilson et al. (2021), pose even greater challenges with shorter observation periods and longer prediction horizons.

**Interactions among agents.** Modeling agent-to-agent interactions involves capturing their behavior over time and space. One popular technique is to use an occupancy map centered at the ego agent's position to map neighboring agents, known as the *agent-centric* or marginal trajectory prediction approach (Wang et al., 2023). This approach provides an invariant translation from a global coordinate system of all agents to the ego agent's local coordinate system, facilitating the interaction modeling using the occupancy map with a fixed ego perspective. Hence, this approach is widely used for data augmentation in trajectory prediction for autonomous vehicles (Varadarajan et al., 2022; Nayakanti et al., 2022; Gu et al., 2021), as well as for pedestrian trajectory prediction (Shi et al., 2023). However, inferring the positions of the neighboring agents through translation to the ego agent's local coordinate system can be time-consuming, as it requires iterating the translation one by one for each agent to be predicted. Another approach is to predict the trajectories of all agents in the scene jointly, which is also called scene-centric approach (Sun et al., 2022). This approach can speed up the inference process significantly but requires handling the variance in the global positions of each agent. Alternatively, interactions among agents are modeled using graph models (Zhang et al., 2019), in which agents are treated as nodes, their connections are modeled as edges, and the interaction information among them is conveyed via message passing.

**Context constraints.** Environmental scene contexts can be used to constrain an agent's movement. For example, convolutional and attention-based approaches can extract contextual information from rasterized data like raster maps and RGB images (Sadeghian et al., 2019; Phan-Minh et al., 2020; Yuan et al., 2021b), or vectorized data like High-Definition (HD) maps (Gao et al., 2020; Gu et al., 2021; Ye et al., 2022). However, maps may not be available or outdated for some areas of interest when a vehicle drives in. Also, the scene context information may only have limited impact on pedestrians who walk freely in open environments or shared spaces (Shi et al., 2023). To make prediction models applicable in any scene context settings, many models predict trajectories without using map information (Cheng et al., 2021b; Yuan et al., 2021b). In this work, we do not include any scene contextual information but focus more on the interactions among agents.

Primary criteria to evaluate a prediction model's performance are prediction errors between the predicted trajectories and the corresponding ground truth trajectories. Fig. 1 shows that many recent studies on trajectory prediction prioritize reducing prediction errors, often

competing to achieve centimeter-scale marginal improvement, while model efficiency (e.g., inference time) can vary from tens to several hundreds of milliseconds. For example, even though ScePT (Chen et al., 2022) adopts a scene-centric encoding, the auto-regressive policy network for modeling interactions among agents significantly slow down the inference speed. Due to the sampling process and auto-regression mechanism, the CVAE-based AgentFormer (Yuan et al., 2021b) is inferior to most of the other models regarding inference speed. In comparison, the graph convolution-based model STAR (Yu et al., 2020) slightly reduces the inference time, but it still takes more than 0.1 s to infer a trajectory for each agent. However, this high latency can limit the usage of complex trajectory prediction models in real-time scenarios, especially for autonomous driving systems that require millisecond-level response. In addition to prediction accuracy, more efficient interaction modeling and inference speed are needed. Therefore, in this paper, we aim to achieve a good balance of prediction performance and inference speed for multi-agent multimodal trajectory prediction.

Specifically, we propose GATraj, a multi-agent trajectory prediction model based on graph and attention mechanisms (Vaswani et al., 2017) that considers both prediction accuracy and inference speed. GATraj takes into account the spatial-temporal dynamics of agents and outputs multimodal trajectories. Attention mechanisms are used to capture agents' dynamics, while a more simplified graph convolutional network (GCN)-based module with message passing (Welling and Kipf, 2017) is employed to model agent-to-agent interactions. In order to speedup the prediction process, this interaction module is implemented in a scene-centric fashion, requiring no further time-consuming translation of the neighboring agent's feature encodings to the ego agent's local coordinate system. Hence, unlike agent-centric models, GATraj can jointly predict all agents' trajectories in the given scene at a higher frequency. Furthermore, different from most sampling-based models with auto-regression (Yuan et al., 2021b; Chen et al., 2022; Yuan and Kitani, 2020; Salzmann et al., 2020b), we employ a Laplacian mixture decoder to predict diverse multimodal trajectories all at once for each agent and a winner-takes-all training strategy to mitigate mode collapse.

The main contributions of our work are as follows:

- We propose an end-to-end multimodal trajectory prediction model, named GATraj, which achieves a good balance of prediction performance and inference speed. It employs an efficient scene-centric GCN module to learn agent-to-agent interactions and an attention module to extract spatial-temporal dynamics.

- GATraj uses a Laplacian Mixture Density Network (MDN) decoder and a winner-takes-all (Makansi et al., 2019) training strategy, which produces more accurate probability estimation for the multimodal prediction than the widely used Gaussian MDN decoder.
- GATraj achieves state-of-the-art prediction performance with significantly higher prediction speed, as demonstrated by testing on the ETH/UCY benchmark datasets for pedestrian trajectories. Additionally, it achieves on-par prediction performance at approximately 100Hz for real-time inference on nuScenes for autonomous driving.

## 2. Related work

In this section, we discuss the development of trajectory prediction for pedestrians and vehicles based on the methods applied for modeling sequential dynamics, interactions, and multimodalities of trajectories.

### 2.1. Modeling motion dynamics as a time sequence

The transition of an agent's motion dynamics, namely the change in speed profile, can be simplified as a temporal sequence of states. Methods such as Kalman Filter (Kalman, 1960), Gaussian Process (Kim et al., 2011), and Markov Models (Kitani et al., 2012) have been commonly used for trajectory prediction. However, these techniques have limited performance when it comes to cope with increased temporal complexity.

In recent years, data-driven models with an encoder-decoder structure have become the dominant approach to trajectory prediction modeling. Specifically, Recurrent Neural Networks (RNNs) (Rumelhart et al., 1986) and their variants Long Short-Term Memories (LSTMs) (Hochreiter and Schmidhuber, 1997) and Gated Recurrent Units (GRUs) (Cho et al., 2014) have been used to gate the information for updating the states in a sequence. Additionally, attention mechanisms (Vaswani et al., 2017), widely used in Natural Language Processing (NLP), have shown their effectiveness in learning complex spatial-temporal interconnections and have been adopted in trajectory prediction. The attention mechanisms guide the interconnections between states, helping to address long time-dependency and complex connectivity problems. These models have achieved state-of-the-art performance on various trajectory prediction benchmarks (Xu et al., 2021; Liu et al., 2021; Gu et al., 2022; Zhou et al., 2022; Ngiam et al., 2022). Alternatively, the history trajectories are stored and later retrieved to identify similar motion dynamics. This history information is later treated as reference in the memory-based model SHENet (Meng et al., 2022) and instance-based model MemoNet (Xu et al., 2022) to guide the predictions in the future.

### 2.2. Modeling interactions among agents

Early works in trajectory prediction often relied on hand-crafted features to model interactions among agents. One of the most influential methods is the Social Force Model (SFM) (Helbing and Molnar, 1995), which applies different forces to determine agents' speed and orientation. These forces include a repulsive force for collision avoidance with obstacles and an attractive force for social connections among agents and goals. Game theoretic models (Johora et al., 2022) have also been used to simulate the negotiations of right-of-way among agent players for decision making. However, due to the complex dynamics in both spatial and temporal domains, these models based on manually selected or designed features often have limited performance in modeling multi-agent interactions and the multimodalities of potential future trajectories.

In recent years, interactions among agents have been modeled by aggregating latent variables learned from each agent's motion dynamics. The pioneering work Social-LSTM (Alahi et al., 2016) explores LSTMs (Hochreiter and Schmidhuber, 1997) to encode pedestrians' motion dynamics into hidden states and a pooling mechanism

to model interactions. Many later works (Xue et al., 2018; Cheng et al., 2021b) have extended this structure by including more features, such as agent-to-agent and agent-to-environment interactions using LSTMs or GRUs (Cho et al., 2014). However, the model performances heavily depend on the hidden states, and with the increase in trajectory length and complexity, the performances are often significantly degraded (Hug et al., 2021).

Attention-based (Vaswani et al., 2017) and graph models, such as Graph Convolutional Networks (GCNs) (Welling and Kipf, 2017), have been leveraged to model agent-to-agent interactions in trajectory prediction. The self- and cross-attention mechanisms have shown their effectiveness in learning interaction information (Yu et al., 2020; Yuan et al., 2021b; Zhu et al., 2021). For instance, AgentFormer (Yuan et al., 2021b) proposes an agent-aware attention mechanism that simultaneously models the temporal and social dimensions among agents. In addition to attention mechanisms, GCNs are widely used to model interactions in trajectory prediction (Zhang et al., 2019; Shi et al., 2020; Gilles et al., 2022; Bae et al., 2022; Shi et al., 2023). Agents are represented as nodes, and their connections are represented as edges, allowing for message passing between nodes to capture interactions between agents. This paper describes an implementation of attention mechanisms to learn salient spatial-temporal features and a GCN module with simplified structure to more efficiently model agent-to-agent interactions.

### 2.3. Multimodal prediction

Multimodal prediction refers to the task of predicting a set of feasible trajectories for each agent, accounting for their stochastic behavior, such as varying speeds and directions. Deep generative models are commonly used to address the multimodality problem, including Generative Adversarial Nets (GANs) (Goodfellow et al., 2014), Variational Auto-Encoder (VAE) (Kingma and Welling, 2014) and its extension Conditional-VAE (CVAE) (Kingma et al., 2014), and Normalizing Flows (Rezende and Mohamed, 2015). Social GAN (Gupta et al., 2018), DESIRE (Lee et al., 2017), and Precog (Rhinehart et al., 2019) are early representative trajectory prediction frameworks that apply these designs, respectively. Recent works such as Cheng et al. (2021a), Yuan et al. (2021b), Lee et al. (2022), Zhou et al. (2023a) and Chen et al. (2022) have extended the CVAE-based design for multimodal trajectory prediction due to its good performance. However, these sampling-based approaches do not provide a straightforward mechanism to estimate the likelihood of each prediction in the random sampling process (Shi et al., 2023). In addition, with the success in computer vision domains, diffusion models (Ho et al., 2020) have been adopted to learn road users' behavior and generate diverse multimodal trajectory predictions (Gu et al., 2022; Mao et al., 2023). However, these models are often time consuming due to the chain of sampling process.

Apart from deep generative models, Mixture Density Networks (MDNs) are proposed to learn a mixture density function, such as Gaussian Mixture Model (GMM), for multimodal trajectory prediction (Salzmann et al., 2020b; Shi et al., 2020; Varadarajan et al., 2022; Deo et al., 2022; Shi et al., 2023). However, most benchmarks only provide a single ground truth trajectory, making it difficult for these models to learn the entire data distribution and generate diverse predictions. This issue, referred to as the mode collapse problem (Richardson and Weiss, 2018), has been a challenge for these methods. The winner-takes-all strategy is proposed to mitigate the mode-collapse problem (Makansi et al., 2019; Zhou et al., 2022; Deo et al., 2022), which only optimizes the loss function of the best predicted modality to facilitate the training process and encourage more diverse predictions.

Inspired by these previous methods, we design our model, GATraj, which uses an encoder-decoder structure to encode past trajectories and interactions, and extract spatial-temporal features through attention mechanisms. In addition, we utilize a GCN to model interactions among agents. Different from the previous models, we seek for a more

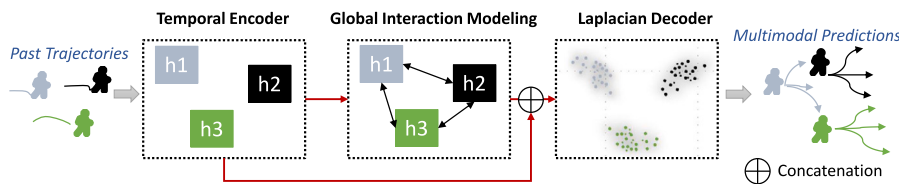


**Fig. 2.** The framework of the proposed model GATraj, consisting of three parts: a Temporal Encoder, a GCN-based global interaction module, and a Laplacian Decoder. It takes as input the observed trajectory of each agent and outputs multimodal predictions of their potential future trajectories.

efficient framework with a scene-centric GCN module to learn global interactions among agents and jointly predict multimodal trajectories of each agent in the given scene simultaneously. This scene-centric GCN module avoids the time-consuming translation into the ego agent's local coordinate system, and significantly speed up the inference process. Rather than relying on a GMM, we introduce a Laplacian Mixture Model (LMM) as the decoder with the winner-takes-all training strategy that generates multiple diverse predictions for each agent. Compared to the recent Mean Location method (Shi et al., 2023) that employs both a GCN module and a GMM decoder for pedestrian trajectory prediction in an ego-centric way, our GATraj achieves joint trajectory prediction in a scene-centric manner and demonstrates that a LMM decoder is more effective than a GMM to model multimodal trajectories.

### 3. Methodology

#### 3.1. Problem formulation

A multi-path trajectory prediction problem is defined as predicting a set of future trajectories  $\{\hat{Y}_{i,1}^{T+1:T+T'}, \dots, \hat{Y}_{i,K}^{T+1:T+T'}\}$  given the observed trajectory  $X_i^{1:T} = \{X_i^1, \dots, X_i^T\}$  of agent  $i$ . Here,  $T$  and  $T'$  denote the total time steps of the observed and the predicted trajectories, respectively;  $T+T'$  is the total sequence length.  $K$  stands for the number of the modes of multiple predicted trajectories.  $X_i^t = \{x_i^t, y_i^t\} \in \mathbb{R}^2$  is the position of agent  $i$  at time step  $t$  in a 2D coordinate system. The formulation can also be easily extended to a 3D coordinate system. To simplify the notation,  $\mathbf{X}$  and  $\mathbf{Y}$  denote the observed and ground truth trajectories, respectively. The loss function aims to reduce the distance between a predicted trajectory  $\hat{\mathbf{Y}}$  and the corresponding ground truth trajectory  $\mathbf{Y}$  for all agents.

The input trajectories are shifted before feeding the trajectory data into the prediction model. Specifically, we follow Cheng et al. (2021a) to use relative positions instead of absolute positions to mitigate domain gaps across different scenes. First, we shift the origin to each agent's last observed time step for data normalization. Then, we use  $\Delta X_i^{2:T} = \{\Delta X_i^2, \dots, \Delta X_i^T\}$  to represent agent  $i$ 's observed trajectory, where  $\Delta X_i^t = \{\Delta x_i^t, \Delta y_i^t\}$  is the offset from  $(t-1)$  to the next time step. However, this shifted representation of trajectories also loses the relative position information between agents, which is essential for modeling their interactions. Hence, we obtain the relative position between agent  $i$  and  $j$  based on their original positions  $(x_i^t - x_j^t, y_i^t - y_j^t)$  at each time step, where  $i \neq j$ . The relative position is further employed in the global interaction modeling.

#### 3.2. The proposed framework

Fig. 2 depicts the overview of our proposed framework GATraj. It consists of three parts: a Temporal Encoder, a GCN-based global interaction module, and a Laplacian Decoder. We first utilize the encoder to extract temporal information of each agent independently and output rich temporal information for the subsequent modules. Then the global interaction module, which employs a GCN adopted from Zhang et al. (2019), aggregates the temporal context of different agents over time and space and updates each agent's hidden state by message passing for interaction modeling. Finally, the learned spatial-temporal feature map is the input of the Laplacian decoder that simultaneously predicts diverse and multimodal future trajectories for all the agents. We explain each part of GATraj in detail in the following.

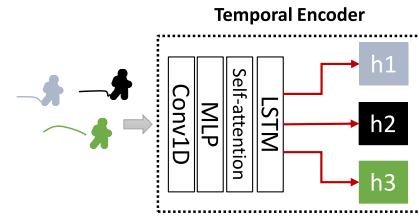


**Fig. 3.** The Temporal Encoder of GATraj. It consists of a sequence of 1D convolution layer (Conv1D) and a two-layer position-wise multilayer perceptron (MLP), a self-attention layer, and an LSTM layer to learn salient temporal features of each agent.

**Temporal encoder.** The self-attention Temporal Encoder learns temporal dynamic information from the observed trajectory. Concretely, as shown in Fig. 3, the temporal encoder takes as input the relative positions  $\Delta X_i^{2:T}$ , which is later passed to a 1D convolution layer (Conv1D) and a two-layer position-wise multilayer perceptron (MLP). In the following, the self-attention layer with three Transformer Encoder blocks (Vaswani et al., 2017) learns salient temporal features — to which time steps of the temporal sequence the encoder should pay more attention through the self-attention layer. Specifically, the default positional encodings of the Transformer network are added at the bottom of the encoder blocks to retain the ordered sequential information. After that, a multi-head of self-attention is applied to jointly attend to the information from different representation subspaces at different positions. Eight heads of self-attention and skip-connections are used in our implementation. Towards the end of the temporal encoder, we utilize an LSTM to extract the temporal dependencies over time. It should be noted that each agent's observed trajectory is considered independently so that their temporal dynamics are processed in parallel.

**Global interaction.** We build a GCN-based module, inspired by SR-LSTM (Zhang et al., 2019), for modeling global interactions among all the concurrent agents in a given scene. SR-LSTM introduces a States Refinement (SR) module to refine the cell state of an LSTM by passing messages among agents at each time step. In contrast, to reduce the computational cost, GATraj only refines cell state once at the latest observed time step but still maintains the ability to model interactions among agents. More specifically, a motion gate and an agent-wise attention (Zhang et al., 2019) are adopted to preserve spatial relationships between the ego agent and its neighbors and to select the most helpful information from neighboring agents for message passing. The cell state output by the LSTM in the Temporal Encoder is updated by a social-aware information selection mechanism as follows:

$$\hat{c}_i^{T,l+1} = \phi_{mp} \left[ \sum_{j \in N(i)} \alpha_{i,j}^{T,l} (g_{i,j}^{T,l} \odot \hat{h}_j^{T,l}) \right] + \hat{c}_i^{T,l}, \quad (1)$$

where  $\hat{c}_i$  denotes agent  $i$ 's cell state after message passing,  $l$  denotes the message passing times,  $\odot$  is the element-wise product operation, and  $\phi_{mp}$  denotes an MLP. Namely, for the ego agent  $i$ , the cell state starts at  $l=0$  with the original output of the LSTM  $c_i$ . All the LSTM hidden states  $\hat{h}_j^{T,l}$  of its neighbors  $j \in N(i)$  are aggregated through the motion gate  $g_{i,j}^{T,l}$ , and the agent-wise attention  $\alpha_{i,j}$  attends to the neighbors based on the agent-to-agent pairwise weights. In addition, a skip connection adds

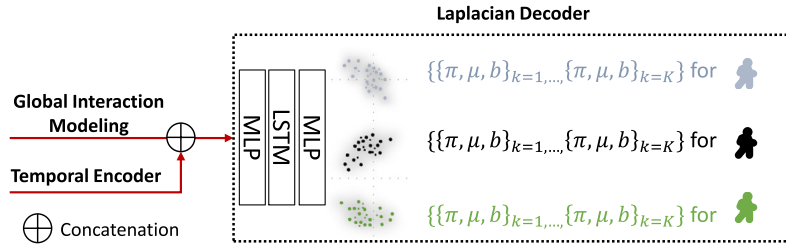


**Fig. 4.** The Laplacian Decoder of GATraj, which consists of a sequence of MLP, LSTM and MLP layers. It takes as input the spatial-temporal dynamic context from the temporal encoder and the GCN module of the global interaction modeling and then outputs a set of parameters, i.e., the likelihood of the mode  $\pi$ , and the location  $\mu$  and scale  $b$  of a Laplacian mixture model for each agent.

agent  $i$ 's previously refined cell  $\hat{c}_i^{T,l}$ . Here, the motion gate is defined by using the relative position between agent  $i$  and  $j$ , and their individual hidden states, as shown in Eqs. (2) and (3),

$$r_{i,j}^{T,l} = \phi_r(x_i^T - x_j^T, y_i^T - y_j^T), \quad (2)$$

$$g_{i,j}^{T,l} = \delta(\phi_m[r_{i,j}^{T,l}, \hat{h}_j^{T,l}, \hat{h}_i^{T,l}]), \quad (3)$$

where  $\phi_m$  and  $\phi_r$  denote MLP and  $\delta$  is the Sigmoid function.

Similarly, another MLP  $\phi_a$  is used to learn the weights  $u_{i,j}^{T,l}$  of the different impacts from the neighbors by Eq. (4). The weights are normalized across all the neighboring agents using the Softmax function denoted by Eq. (5),

$$u_{i,j}^{T,l} = \phi_a[r_{i,j}^{T,l}, \hat{h}_j^{T,l}, \hat{h}_i^{T,l}], \quad (4)$$

$$\alpha_{i,j}^{T,l} = \frac{\exp(u_{i,j}^{T,l})}{\sum_{s \in N(i)} \exp(u_{i,s}^{T,l})}. \quad (5)$$

The hidden state of agent  $i$  then is updated using Eq. (6) after the cell state  $\hat{c}_i^{T,l+1}$  is refined by the above message passing.

$$\hat{h}_i^{T,l+1} = \hat{h}_i^{T,l} + \tanh(\hat{c}_i^{T,l+1}), \quad (6)$$

where  $\tanh$  stands for the hyperbolic tangent function. Different from SR-LSTM, we use a skip-connection to avoid the vanishing gradient problem and discard the output gate for a lightweight structure. Compared to the original GCNs (Welling and Kipf, 2017) that use an adjacency matrix to compute the normalization constant, our agent-wise attention uses learnable MLP  $\phi_r$  and  $\phi_a$  to aggregate relative spatial positional information between the ego and all its neighboring agents and emphasize important neighbors using the attention mechanism to guide the message passing. Moreover, as the interactions among agents are automatically learned by using the above message passing and the agent-wise attention mechanism, there is no further need to translate the neighboring agent's feature encodings to the ego agent's local coordinate system. This significantly reduces the processing time.

**Laplacian decoder.** We introduce a Laplacian MDN decoder to generate future multimodal trajectories, accounting for each agent's stochastic behavior, as shown in Fig. 4. The decoder takes as input the spatial-temporal dynamic context from the temporal encoder and the GCN module of the global interaction modeling. Its outputs are a set of different modes of the predicted trajectory distribution. Concretely, the predicted set of potential trajectories is  $\{\{\pi, \mu, b\}_{k=1}, \dots, \{\pi, \mu, b\}_{k=K}\}$  with a total of  $K$  modes. For mode  $k$ ,  $\pi$  stands for the estimated likelihood of this mode among all the potential modes and  $\sum_{k=1}^K \pi_k = 1$ . In the Laplace distribution of the predicted mode,  $\{\mu, b\} \in \mathbb{R}^{T_f \times 2}$ , the location  $\mu$  and scale  $b$  parameters represent the mean positions and standard deviations of the predicted trajectory, respectively. To simplify the generation of each trajectory, in this paper, we use the sequence of the mean positions  $\mu$  as the predicted trajectory.

To be more specific, in the decoding process, the decoder takes as input the hidden state  $h_i^T$  of the LSTM from the Temporal Encoder and the hidden state  $\hat{h}_i^{T,l+1}$  and cell state  $\hat{c}_i^{T,l+1}$  after the message

passing with the GCN module.  $\{h_i^T, \hat{h}_i^{T,l+1}, \hat{c}_i^{T,l+1}\} \in \mathbb{R}^{N \times D}$ , where  $D$  is the dimension of the embedded feature space and  $N$  is the total number of agents in the current scene. First, an MLP projects the shape of the input into  $[K, N, D]$ , where  $K$  is the number of modes to be predicted. With projected feature embeddings, we utilize an MLP and a Softmax function to learn the probability  $\hat{\pi}_{i,1:K}$  of each mode for each agent. Then, an LSTM decodes the aggregated and embedded hidden states into a shape of  $[K \times N, T', D]$ , recovering the prediction time-step dimension  $T'$ . It should be noted that here we simultaneously predict all the time steps using the hidden states instead of applying a step-wise auto-regressing to further speed up the prediction. We empirically found that using LSTM contributes to a more efficient gating of the sequential information over the time axis (more details in Section 4.6). Finally, two side-by-side MLPs predicts a mixture of Laplace distribution with  $K$  modes of the potential future trajectories for each agent, i.e., the location  $\hat{Y}_{i,1:K} \in \mathbb{R}^{K \times T' \times 2}$  and its associated scale  $\hat{b}_{i,1:K} \in \mathbb{R}^{K \times T' \times 2}$ , and  $\hat{\pi}_{i,1:K} \in \mathbb{R}^K$ .

### 3.3. Loss function

The total loss of GATraj is decoupled into two parts - *regression loss* and *classification loss*. We utilize a Winner-Takes-All strategy (Makansi et al., 2019) for the supervision by each agent's single ground truth trajectory to encourage GATraj to generate diverse predictions. Namely, for the regression loss, we only optimize the best mode  $k^*$  of the  $K$  predictions during training instead of the weighted strategy by an Expectation-Maximization algorithm for a GMM. Following Zhou et al. (2022), we employ the negative log-likelihood for the Laplace distribution as the regression loss and the cross-entropy loss as the classification loss for the mode optimization,

$$k^* = \arg \min_{k \in K} \|\hat{Y}_{i,k} - Y_i\|^2, \quad (7)$$

$$\mathcal{L}_{\text{reg},i} = \frac{1}{T'} \sum_{t=T+1}^{T+T'} -\log P(Y_i^t | \hat{Y}_{i,k^*}^t, \hat{b}_{i,k^*}^t), \quad (8)$$

$$\mathcal{L}_{\text{cls},i} = \sum_{k=1}^K -\pi_{i,k} \log(\hat{\pi}_{i,k}), \quad (9)$$

where  $\log P(\cdot | \cdot)$  is the logarithmic probability density function of the Laplace distribution.  $\hat{\pi}_{i,k}$  is the predicted probability, and  $\pi_{i,k}$  is our target probability. We employ a soft displacement error adopted from Zhou et al. (2022) as our target probability.

## 4. Experiments

### 4.1. Datasets

The benchmarks ETH/UCY (Pellegrini et al., 2009; Lerner et al., 2007) and nuScenes (Caesar et al., 2020) are used to train and test the performance of our proposed model. ETH/UCY contains thousands of pedestrian trajectories sampled in 2.5 Hz in five different datasets, i.e., Eth, Hotel, Uni, Zara1, and Zara2. The time horizon lets the model

observe eight steps and predict the subsequent 12-step trajectories. We follow the standard leave-one-out training and test partitioning, in order to test the model's generalization performance in unseen scenes. Concretely, four of the five datasets are used for training, and the left-out one is for the test. This partitioning is iterated for each dataset. The nuScenes prediction task provides separate training and test sets for vehicle trajectory prediction. In total, nuScenes includes 1000 driving scenarios in different cities. Each scenario contains various neighboring agents and the target vehicles for the motion prediction task. In this dataset, a trajectory is sampled in 2 Hz. The model observes up to four-time steps and predicts the following 12-step trajectories. We use the provided data partitioning, namely, 750 scenarios for training, 150 scenarios for validation, and the remaining 150 scenarios for testing.

In this work, we adhere to the default settings of the parameter mode  $K$ , as recommended by the datasets. Specifically,  $K$  is set to 20 for predicting multiple trajectories on the ETH/UCY datasets for pedestrians, as pedestrians have greater freedom of movement in open spaces. For the nuScenes dataset, which involves predicting vehicle trajectories,  $K$  is set to 5 and 10 to align with the official benchmark setting for the evaluation. Compared to pedestrians, this distinction of  $K$  for vehicles is made because vehicles are more constrained by lane boundaries.

#### 4.2. Evaluation metrics

We apply the two most commonly used metrics, Average Displacement Error (ADE) and Final Displacement Error (FDE) in meters, to evaluate trajectory prediction accuracy. ADE measures the Euclidean distance between the predicted and ground truth trajectories and is averaged at each position for each agent. FDE is the Euclidean distance of the last position between the predicted and ground truth trajectories.

$$\text{ADE}_K = \frac{1}{N} \frac{1}{T'} \min_{k=1}^K \sum_{i=1}^N \sum_{t=T+1}^{T+T'} \|\hat{y}_{i,k}^t - y_i^t\|^2, \quad (10)$$

$$\text{FDE}_K = \frac{1}{N} \min_{k=1}^K \sum_{i=1}^N \|\hat{y}_{i,k}^{T+T'} - y_i^{T+T'}\|^2, \quad (11)$$

where  $N$  is the total number of agents. Here,  $K$  denotes that we generate  $K$  predictions for each agent and report the best one measured by ADE and FDE, respectively.

Moreover, to evaluate the performance of the predicted distribution of a mixture model, we use negative log-likelihood (NLL) to compare the likelihood estimation across different models tested on the same data. We report the average NLL and standard deviation across all the agents.

#### 4.3. Baselines

We compare the performance of GATraj with a variety of recent state-of-the-art models in the competition on the popular pedestrian datasets and the dataset for autonomous driving introduced in Section 4.1. To ensure a fair comparison, we exclusively benchmark our model, GATraj, against multi-path trajectory prediction models on both the ETH/UCY and nuScenes datasets. Our focus remains on models that do not leverage map information in the nuScenes test set for autonomous driving.

In general, we classify the baseline models according to their primary network architectures, as outlined in Table 1. It is worth noting that some of the baseline models also incorporate multiple network architectures.

#### 4.4. Experimental setting

The hyper-parameters of GATraj are as follows. The hidden states and the embedding dimensions are all set to 64. We apply the Adam

**Table 1**  
The list of baseline models.

Architecture	Model
CNN-based	MTP ( <a href="#">ICRA'19</a> ) ( <a href="#">Cui et al., 2019</a> ), CoverNet ( <a href="#">CVPR'20</a> ) ( <a href="#">Phan-Minh et al., 2020</a> )
GAN-based	Social GAN ( <a href="#">CVPR'18</a> ) ( <a href="#">Gupta et al., 2018</a> ), SoPhiE ( <a href="#">CVPR'18</a> ) ( <a href="#">Sadeghian et al., 2019</a> )
CVAE-based	DLow-AF ( <a href="#">ECCV'20</a> ) ( <a href="#">Yuan and Kitani, 2020</a> ), Trajectron++ ( <a href="#">ECCV'20</a> ) ( <a href="#">Salzmann et al., 2020b</a> )
GCN-based	SGCN ( <a href="#">CVPR'21</a> ) ( <a href="#">Shi et al., 2021</a> ), PGP ( <a href="#">CoRL'22</a> ) ( <a href="#">Deo et al., 2022</a> ) Social-BIGAT ( <a href="#">Neurips'21</a> ) ( <a href="#">Kosaraju et al., 2019</a> ), ScePT ( <a href="#">CVPR'22</a> ) ( <a href="#">Chen et al., 2022</a> ), GP-Graph ( <a href="#">ECCV'22</a> ) ( <a href="#">Bae et al., 2022</a> ) FRM ( <a href="#">ICLR'23</a> ) ( <a href="#">Park et al., 2023</a> )
Transformer with attention-based	STAR ( <a href="#">ECCV'20</a> ) ( <a href="#">Yu et al., 2020</a> ), AgentFormer ( <a href="#">ICCV'21</a> ) ( <a href="#">Yuan et al., 2021b</a> ), MemoNet ( <a href="#">CVPR'22</a> ) ( <a href="#">Xu et al., 2022</a> ), SHENet ( <a href="#">Neurips'22</a> ) ( <a href="#">Meng et al., 2022</a> ), EqMotion ( <a href="#">CVPR'23</a> ) ( <a href="#">Xu et al., 2023</a> )
Mixture Models	MultiPath ( <a href="#">CoRL'20</a> ) ( <a href="#">Chai et al., 2020</a> ), MeanLocation ( <a href="#">PAMI'23</a> ) ( <a href="#">Shi et al., 2023</a> )
Diffusion-based	MID ( <a href="#">CVPR'22</a> ) ( <a href="#">Gu et al., 2022</a> ), LED ( <a href="#">CVPR'23</a> ) ( <a href="#">Mao et al., 2023</a> )
Other models	The flow-based LDS-AF ( <a href="#">ICCV'21</a> ) ( <a href="#">Ma et al., 2021</a> ), The clustering-based PCCSNet ( <a href="#">ICCV'21</a> ) ( <a href="#">Sun et al., 2021</a> ), The energy-based model LB-EBM ( <a href="#">CVPR'22</a> ) ( <a href="#">Pang et al., 2021</a> )

**Table 2**  
The quantitative results on nuScenes ([Caesar et al., 2020](#)).

Model	Map info.	ADE <sub>5</sub>	FDE <sub>5</sub>	ADE <sub>10</sub>	FDE <sub>10</sub>
DLow-AF ( <a href="#">Yuan and Kitani, 2020</a> )	No	2.11	4.70	1.78	3.58
LDS-AF ( <a href="#">Ma et al., 2021</a> )	No	2.06	4.62	1.65	3.50
AgentFormer ( <a href="#">Yuan et al., 2021b</a> )	No	1.97	4.21	1.58	3.14
MTP ( <a href="#">Cui et al., 2019</a> )	Yes	2.93	–	2.93	–
MultiPath ( <a href="#">Chai et al., 2020</a> )	Yes	2.32	–	1.96	–
CoverNet baseline ( <a href="#">Caesar et al., 2020</a> )	Yes	1.96	–	1.48	–
Trajectron++ ( <a href="#">Salzmann et al., 2020b</a> )	Yes	1.88	–	1.51	–
AgentFormer ( <a href="#">Yuan et al., 2021b</a> )	Yes	1.86	3.89	1.45	2.86
PGP ( <a href="#">Deo et al., 2022</a> )	Yes	1.27	–	0.94	–
FRM ( <a href="#">Park et al., 2023</a> )	Yes	1.18	–	0.88	–
GATraj (Ours)	No	1.87	4.08	1.46	2.97

optimizer ([Kingma and Ba, 2015](#)) with a learning rate of  $5e^{-4}$  and a cosine annealing schedule until it reaches  $1e^{-5}$ . The batch size is set to 32, and the maximum epoch is set to 1000. On ETH/UCY, the maximum distance of the ego and neighboring agents is set to 10 m and the GCN layers for messaging passing are set to  $l = 2$ . On nuScenes, given the faster driving speed of vehicles and fewer neighboring agents than ETH/UCY, the maximum distance of the ego and neighboring agents is set to 100 m and the GCN layers for messaging passing are set to  $l = 1$ . Our code is released at <https://github.com/mengmengliu1998/GATraj> with more detailed settings.

#### 4.5. Results

##### 4.5.1. Quantitative results

First, we present the quantitative prediction results on the nuScenes benchmark. As the map context information is a strong prior to constrain vehicle trajectories driving on the lane of road ([Caesar et al., 2020](#)), we compare our model to the other models without any map information and with map information, separately. As shown in Table 2, our model GATraj achieves the best performance measured by ADE and FDE in predicting five and ten trajectories for each agent,

**Table 3**

Quantitative results on ETH/UCY (Pellegrini et al., 2009; Lerner et al., 2007) measured by ADE<sub>20</sub>/FDE<sub>20</sub>. The best/2nd best performances are indicated in boldface and underline.

Models	Eth	Hotel	Uni	Zara1	Zara2	Avg
Social GAN (Gupta et al., 2018)	0.81/1.52	0.72/1.61	0.60/1.26	0.34/0.69	0.42/0.84	0.58/1.18
SoPhie (Sadeghian et al., 2019)	0.70/1.43	0.76/1.67	0.54/1.24	0.30/0.63	0.38/0.78	0.54/1.15
Social-BIGAT (Kosaraju et al., 2019)	0.69/1.29	0.49/1.01	0.55/1.32	0.30/0.62	0.36/0.75	0.48/1.00
Trajectron++ (Salzmann et al., 2020b)	0.67/1.18	0.18/0.28	0.30/0.54	0.25/0.41	0.18/0.32	0.32/0.55
SGCN (Shi et al., 2021)	0.63/1.03	0.32/0.55	0.37/0.70	0.29/0.53	0.25/0.45	0.37/0.65
STAR (Yu et al., 2020)	0.36/0.65	0.17/0.36	0.31/0.62	0.26/0.55	0.22/0.46	0.26/0.53
AgentFormer (Yuan et al., 2021b)	0.45/0.75	0.14/0.22	0.25/0.45	0.18/0.30	0.14/0.24	0.23/0.39
MID (Gu et al., 2022)	0.39/0.66	0.13/0.22	0.22/0.45	0.17/0.30	0.13/0.27	0.21/0.38
LB-EBM (Pang et al., 2021)	0.30/0.52	0.13/0.20	0.27/0.52	0.20/0.37	0.15/0.29	0.21/0.38
PCCSNet (Sun et al., 2021)	0.28/0.54	0.11/0.19	0.29/0.60	0.21/0.44	0.15/0.34	0.21/0.42
ScePT (Chen et al., 2022)	0.10/0.65	0.13/0.77	0.12/0.65	0.13/0.77	0.14/0.81	0.12/0.73
MemoNet (Xu et al., 2022)	0.40/0.61	0.11/0.17	0.24/0.43	0.18/0.32	0.14/0.24	0.21/0.35
GP-Graph (Bae et al., 2022)	0.43/0.63	0.18/0.30	0.24/0.42	0.17/0.31	0.15/0.29	0.23/0.39
SHENet (Meng et al., 2022)	0.41/0.61	0.13/0.20	0.25/0.43	0.21/0.32	0.15/0.26	0.23/0.36
MeanLocation (Shi et al., 2023)	0.29/0.49	0.12/0.18	0.29/0.51	0.20/0.35	0.15/0.27	0.21/0.35
EqMotion (Xu et al., 2023)	0.40/0.61	0.12/0.18	0.23/0.43	0.18/0.32	0.13/0.23	0.21/0.35
LED (Mao et al., 2023)	0.39/0.58	0.11/0.17	0.26/0.43	0.18/0.26	0.13/0.22	0.21/0.33
GATraj (Ours)	<u>0.26/0.42</u>	<b>0.10/0.15</b>	<u>0.21/0.38</u>	<u>0.16/0.28</u>	<u>0.12/0.21</u>	<u>0.17/0.29</u>

compared to the CVAE-based models DLow-AF and AgentFormer w/o map information, as well as the flow-based model LDS-AF. GATraj reduces the prediction errors around ten centimeters compared to the runner up model AgentFormer w/o map information. Interestingly, when comparing GATraj with the map-based models, it still maintains a relatively good level of prediction performance. For example, it surpasses the convolutional-based baseline CoverNet with a clear margin and performs slightly better than the CAVE-based Trajectron++ with scene context information to constrain the predictions. Moreover, GATraj only marginally falls behind AgentFormer measured in ADE, even though the latter benefits largely by including the scene information. Nevertheless, due to the lack of map information, such as lane boundaries and traffic rules extracted from a vectorized HD map, GATraj falls behind the recent HD-map based models PGP (Deo et al., 2022) and FRM (Park et al., 2023). More discussion about the limitation of missing map information can be found in Section 4.6.1

Next, we present the quantitative prediction results on ETH/UCY. Different from the nuScenes dataset with most of the agents being vehicles, the agents in the ETH/UCY datasets are all pedestrians. As shown in Fig. 6, pedestrians move freely because the scenes depicted in ETH/UCY consist of open spaces with few constraints on the movements of pedestrians. Therefore, in these datasets, only a few models make use of scene information, such as SoPhie and ScePT. To simplify the comparison, we compare GATraj with the other models in Table 3 without differentiating the inclusion of scene information.<sup>2</sup>

Overall, our model achieves the best performance measured in both ADE and FDE on Hotel and Zara2, and the best FDE on Eth, Uni and the average FDE across the datasets for predicting 20 trajectories for each agent. It achieves the second best on the other datasets, slightly falling behind ScePT in terms of ADE on Eth, Uni, and the average ADE across the datasets. ScePT uses a conditional policy learning to decode scene-consistent predictions to reduce the average prediction errors, whereas GATraj only conditions on the observed trajectories for prediction. In addition, due to the auto-regressive policy and the partitioning of the scene-graph into cliques, ScePT requires significantly much longer computational time (see Table 4). Compared to the most recent diffusion-model based predictor LED, the performance of GATraj is superior on most datasets, except on Zara1 in terms of FDE.

Furthermore, Fig. 1 and Table 4 show the comparison of the model size, training time, and prediction speed between our model and the models with similar prediction performance. It is evident that, in

<sup>2</sup> The results of Trajectron++ and AgentFormer are updated according to implementation issue #53 (Salzmann et al., 2020a) and issue #5 (Yuan et al., 2021a), respectively.

comparison to the other models, GATraj is of medium size and can be trained using a single GPU in just over one day, which is much easier to train than the other models such as AgentFormer (Yuan et al., 2021b), ScePT (Chen et al., 2022), and ProphNet (Wang et al., 2023).

Because the settings of the model across the datasets are similar, we conduct an experiment on Zara2 (Lerner et al., 2007) using a single Tesla V100 GPU and a batch size of 32 to demonstrate the inference speed. Our full model demonstrates an almost three-times faster prediction speed (*i.e.*, 10.1 ms vs. 29.1 ms) than the 2nd fastest model Trajectron++. Due to the lack of released code, we employ a linear function to estimate the fastest agent-centric model ProphNet's inference speed for a batch size of 32 and a time horizon of 12 steps in Table 4. It can be seen that GATraj has a much lower latency than ProphNet. Moreover, to ensure a more equitable comparison, we aligned the batch size for GATraj at 64 and the time horizon at 30 steps, matching the settings reported for ProphNet in the original paper. The average inference speed of GATraj stands at 1.7 ms per agent, significantly outperforming ProphNet's 28 ms per agent. The following factors contribute to this computational difference: First, GATraj takes a scene-centric approach, concurrently predicting the trajectories of all agents within the same scene. Conversely, ProphNet employs an agent-centric methodology that necessitates the normalization of trajectories to each agent's local coordinate system. Second, ProphNet employs multiple hydra heads as an ensemble strategy and utilizes non-maximum suppression to consolidate all predicted trajectories into a final output. These steps introduce additional latency to the overall inference speed.

In addition, by removing the GCN-based interaction module and the attention mechanisms, our model can reach a speed of 3.9 ms, and the size of our model is also decreased from 276 K to 183 K. Later, we will demonstrate that even without the GCN and attention mechanisms, our model maintains a relatively good prediction accuracy, as shown in Tables 7 and 8.

#### 4.5.2. Qualitative results

In the following, we present the visualization of the prediction results by GATraj on nuScenes for autonomous driving and ETH/UCY for pedestrian trajectories.

To demonstrate the capability of predicting multimodal trajectories of the target vehicle in nuScenes, we visualize ten potential trajectories ( $K = 10$ ) in each scenario, as shown in Fig. 5. GATraj generates diverse multimodal predictions for the target vehicle, such as: turning into different directions while approaching the intersection in (a) and (b), driving through the intersection in (c), and moving at different speeds while passing a straight road in (d).

**Table 4**

Model efficiency in terms of number of parameters, training time, and inference speed with a batch size of 32. The best performance is in boldface.

Models	# Params (K)	GPU training time	Inference (ms)
STAR (Yu et al., 2020)	965	1 × A40, 27H	123.2
Trajectron++ (Salzmann et al., 2020b)	<b>126</b>	2 × GTX1080Ti, 8H	29.1
AgentFormer (Yuan et al., 2021b)	592	1 × RTX2080Ti, 72H	133.3
PCCSNet (Sun et al., 2021)	347	1 × RTX2080Ti, 9H	81.3
ScePT (Chen et al., 2022)	139	2 × A40, 100H	566.3
ProphNet (Wang et al., 2023)	7314	16 × V100, 22H	358
GATraj (Ours) w/o GCN, SA	183	1 × A40, 21H	<b>3.9</b>
GATraj (Ours) w/o GCN	259	1 × A40, 23H	6.6
GATraj (Ours)	276	1 × A40, 30H	10.1

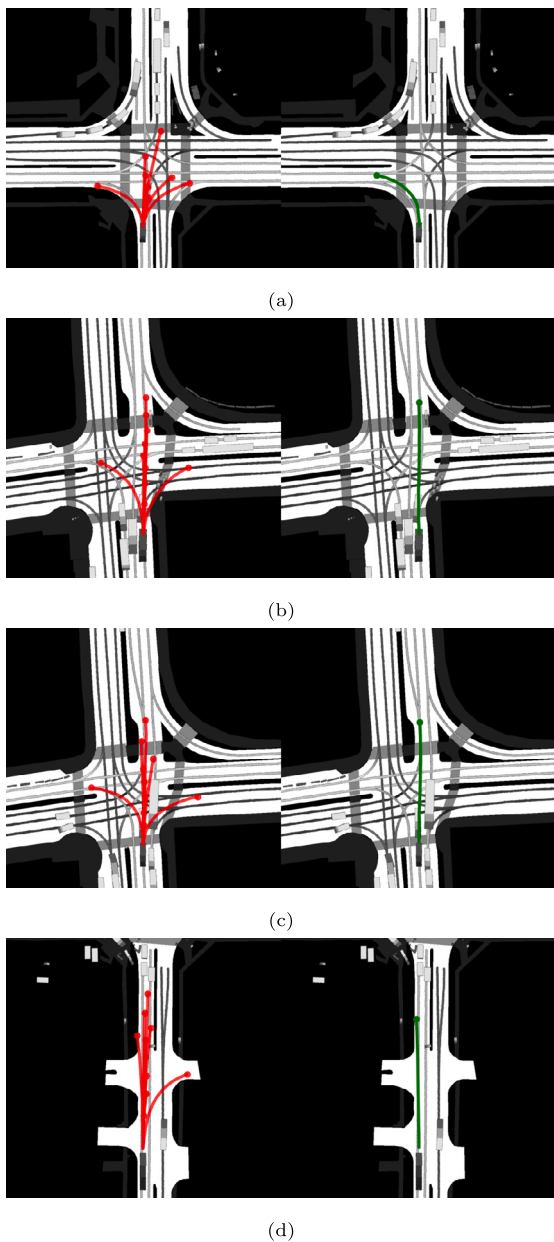


**Fig. 5.** Qualitative results of GATraj on the nuScenes (Caesar et al., 2020) dataset. Left: predictions, right: the ground truth. The observed trajectory is denoted as dark rectangles with descending grayscale along the time steps – a darker color indicates an earlier time step. The prediction is in red dotted lines, and the corresponding ground truth is in green dotted lines. The HD map is only used for visualization and not used as extra contextual information for prediction. (For interpretation of the references to color in this figure legend, the reader is referred to the web version of this article.)

As pedestrians move closely with each other in ETH/NYC, in Fig. 6, we first only plot the best prediction of 20 trajectories ( $K = 20$ ) for each pedestrian for clear visualization. The first row shows the scenarios in ETH. GATraj correctly predicts a pedestrian walking diagonally in the passage way and another pedestrian turning around to the street in (a). It also correctly predicts pedestrians walking in parallel in a small group (two pedestrians) in (b) and a big group (five pedestrians) in (c). Similarly, even though pedestrians move at various speeds, we can see that the predictions of GATraj are well aligned with the ground truth trajectories, especially for the final positions, in the second row for the scenarios in Hotel and the third row for the scenarios in Uni. Interestingly in (i), GATraj can generate reasonable non-linear predictions, such as turning around or changing direction suddenly. The last row shows the predictions of the scenarios in Zara01/02. GATraj demonstrates that it can generate good predictions for multiple pedestrians walking closely to each other, and it also correctly predicts a pedestrian curving around a parked vehicle in (k).

Furthermore, in Fig. 7, we showcase the multimodal predictions for pedestrian trajectory prediction, i.e., 20 trajectories for each pedestrian. It can be observed from the predictions that GATraj is capable of generating highly diverse predictions in terms of moving direction and speed. It is intriguing to note that some of the predictions capture potential intentions of the pedestrian. For instance, in (b), certain predictions indicate the tram station along the road, and one prediction even suggests that the pedestrian might turn around. Similarly, in (d), one prediction points towards the shop window, while other predictions indicate different directions as the pedestrian moves further into the intersection of the road.

#### 4.6. Ablation studies

In this subsection, we carry out a series of ablation studies to provide a comprehensive insight of GATraj's performance.

First, we start with analyzing the performance of the Laplacian MDN decoder (LMM). We compare it with a Gaussian MDN decoder (GMM) using negative log-likelihood for the multimodal predictions. Both decoders use the same layers of neural network, except for the parameterization of the outputted distributions.

As shown in Fig. 8, it is clear that the LMM decoder achieves a much lower negative log-likelihood (NLL) than the GMM decoder for predicting both ten modes ( $K = 10$ ) and five modes ( $K = 5$ ) on nuScenes for vehicle trajectory prediction. the LMM decoder also achieves evidently lower NLL across all the datasets in ETH/UCY for pedestrian trajectory prediction with 20 modes (see Fig. 9).

Moreover, Tables 5 and 6 show the comparison of the predictions errors measured by ADE and FDE on nuScenes and ETH/UCY, respectively, between GMM and LMM using the same network configuration except for the outputted distributions. Both tables clearly show that the LMM decoder generates better predictions measured in lower ADE and FDE on each dataset.

To summarize, these consistently better results in terms of NLL and prediction errors of LMM compared to GMM validate that the LMM

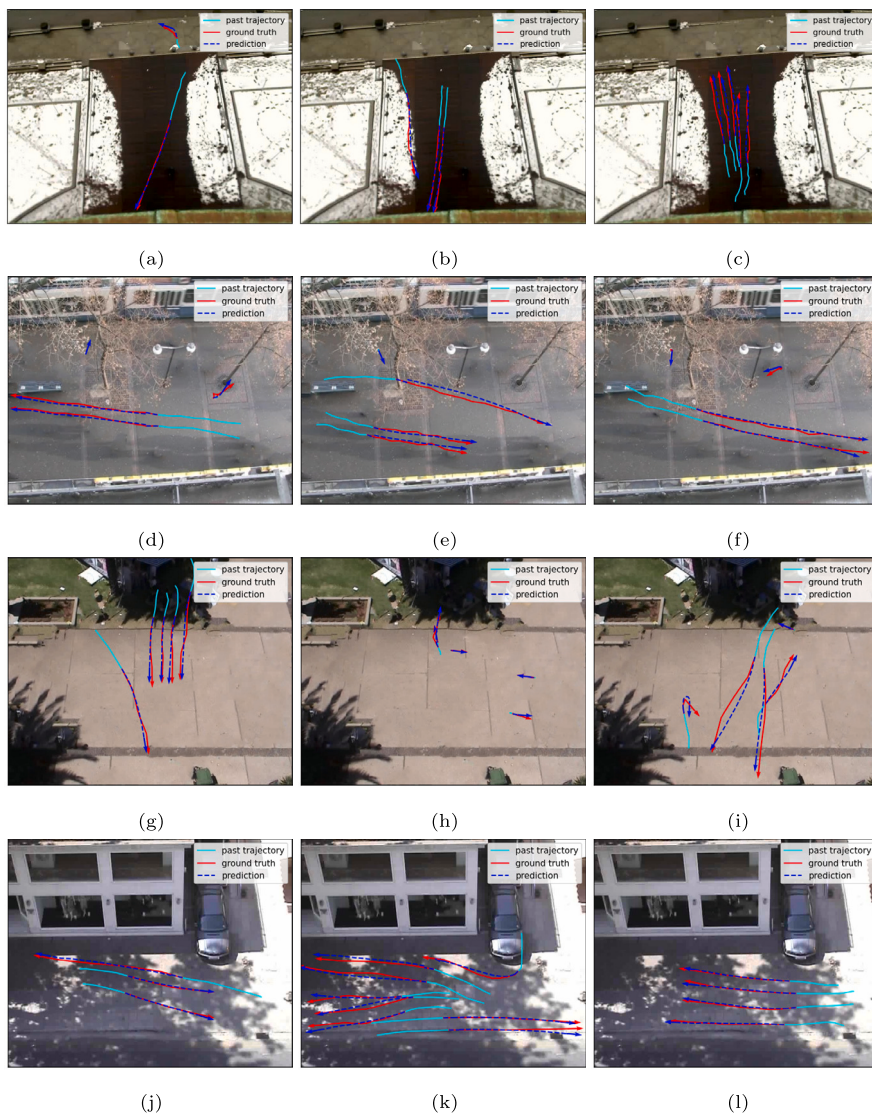


**Fig. 6.** Qualitative results tested on the ETH/UCY (Pellegrini et al., 2009; Lerner et al., 2007) datasets. From the first row to the forth rows, they are the scenarios in Eth, Hotel, Uni, and Zara1/2.

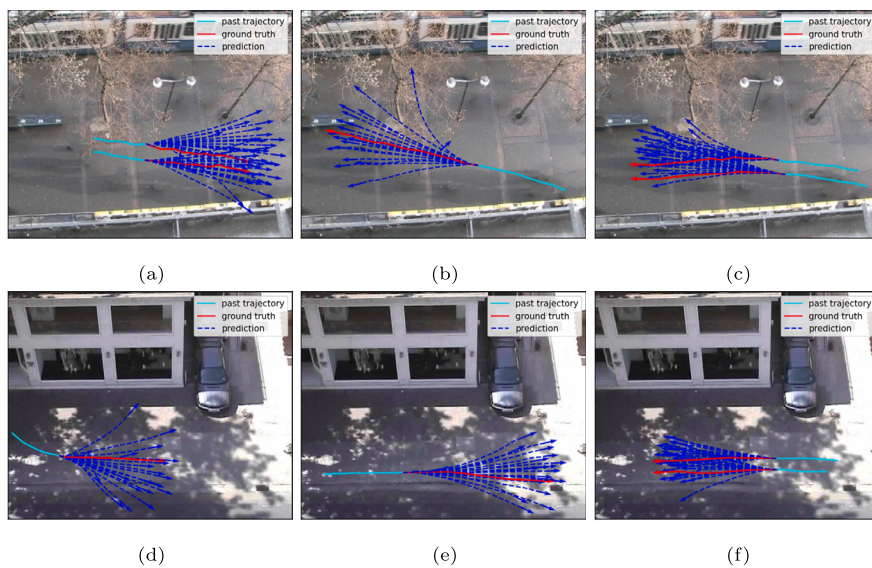


**Fig. 7.** Qualitative results with multimodal predictions tested on the ETH/UCY (Pellegrini et al., 2009; Lerner et al., 2007) datasets.

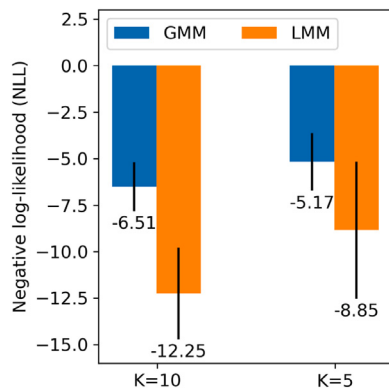


**Fig. 8.** The negative log-likelihood (NLL) between LMM and GMM tested on nuScenes. The error bars stand for the standard deviations.

**Table 5**

The comparison of the prediction errors between LMM and GMM on nuScenes.

Decoder	$ADE_5$	$FDE_5$	$ADE_{10}$	$FDE_{10}$
GMM	2.08	4.67	1.64	3.45
LMM	2.00	4.46	1.57	3.28

**Table 6**

The comparison of the prediction errors (ADE/FDE) between LMM and GMM on ETH/UCY.

Models	Eth	Hotel	Uni	Zara1	Zara2	Avg.
GMM	0.27/0.47	0.11/0.18	0.22/0.40	0.18/0.34	0.12/0.23	0.18/0.32
LMM	0.26/0.42	0.10/0.15	0.21/0.38	0.16/0.28	0.12/0.21	0.17/0.29

**Table 7**

The ablation study of the self-attention (SA) mechanism and the GCN module on nuScenes.

SA	GCN	$ADE_5$	$FDE_5$	$ADE_{10}$	$FDE_{10}$
–	–	2.00	4.45	1.57	3.29
✓	–	2.00	4.46	1.57	3.28
✓	✓	1.87	4.08	1.46	2.97

decoder is more accurate in estimating the probability of multimodal predictions.

Next, we conduct the ablation study to analyze the effectiveness of the self-attention mechanism (SA) to enhance the learning of spatial-temporal information and the GCN module to model interactions among agents. The effectiveness of the self-attention mechanisms is not so obvious on nuScenes (as shown in Table 7), while the model's performance decreases without the self-attention mechanisms on ETH/UCY (as shown in Table 8). The reason could be that nuScenes only lets the model observe a short trajectory, *i.e.*, from two to four-time steps, while ETH/UCY provides eight-time steps for observation; The self-attention mechanisms may work better on longer sequences. After removing the GCN module, the performance drops clearly on both datasets.

In addition, we substitute the LSTM layer by an MLP layer in the decoder to analyze the effect of the hidden states in the LSTM for temporal information. It can be seen from Tables 9 and 10, replacing the LSTM layer with an MLP in the decoder leads to an apparent decrease in performance on both nuScenes and ETH/UCY.

In the following, we investigate the effect of different trajectory inputs, namely, position sequences and offset sequences. As shown in Tables 11 and 12, our model using offset sequences achieves better performance than position sequences on ETH/UCY, but similar performance on nuScenes. Our conjecture is that the offset sequences are less sensitive to the absolute position in a given scene and using the offset sequences can mitigate the domain gaps across different scenes. It explains why we observe a clear performance drop when

substituting the offset sequences by the position sequences in testing on the ETH/UCY datasets using the leave-one-out cross validation. In addition, combining both position and offset sequences yield similar performances as that of using the offset sequences alone, leading to no joint benefit. Therefore, based on the empirical findings, we decide to use the offset sequences as the trajectory input of our model for trajectory prediction.

Different from the ETH/UCY datasets that only contain pedestrian road users, the nuScenes dataset contains a mixture of vehicle types. To explore the impact of road user types on prediction performance, we conduct an additional ablation study by incorporating road user type information into the training of the GATraj model on the nuScenes dataset. Specifically, the target vehicles to be predicted in the test set are further categorized into types such as *bus*, *car*, *truck*, *emergency vehicle*, and *construction vehicle*. Firstly, as demonstrated in Table 13, prediction performance for buses, cars, and trucks exhibits slight variations. These vehicle types are commonly observed and share similar driving behaviors. However, prediction errors for emergency vehicles, such as ambulances and police cars, are notably larger than those of the others. This type of vehicles only accounts for less than 1% of the total vehicles, making the data samples very unbalanced. Also, the disparity of prediction performance arises from emergency vehicles having priority over other vehicles and traffic signals, and their ability to travel at higher speeds to interact with other road users in a larger range, introducing a greater challenge for prediction. In contrast, construction vehicles are usually constrained to lower speeds, making their trajectories easier to predict compared to the other types. Secondly, it is evident that the errors for  $K = 10$  are smaller than those for  $K = 5$ , indicating that a larger  $K$  can more precisely capture the uncertain driving patterns across all vehicle types. The performance difference with respect to the mode number  $K$  is particularly significant, especially for emergency vehicles. This is because emergency vehicles on duty are frequently driving hastily and can abruptly disrupt the normal traffic flow, thereby making their behavior more uncertain. Consequently, additional modalities might be necessary to effectively capture the uncertain driving behavior of emergency vehicles. It is also interesting to observe that with the incorporation of vehicle types, the average performance for  $K = 5$  is slightly better than that without this type of information. For instance,  $FDE_5$  reduces from 4.08 to 4.02 (see Table 2). While the performance difference for  $K = 10$  is relatively small, e.g.  $FDE_5$  slightly increases from 2.97 to 3.00. Our conjecture is that with a larger number of modalities, the model can already capture an agent's behavior effectively without requiring knowledge of its vehicle type.

We further analyze the performance of GATraj by increasing the number of components. The results shown in Fig. 10 demonstrate that increasing the number of components of the MDN decoder evidently leads to a gain in prediction accuracy. This trend indicates that the Laplacian MDN decoder can generate diverse multimodal predictions. However, many benchmarks limit the maximum number of predictions for each agent, *i.e.*, ETH/UCY recommends 20, and nuScene only allows up to ten predictions for each agent. The limited computational resources of real-time applications may only allow a small number of predictions as well. Some recent works, such as Chai et al. (2020) and Wang et al. (2023), have explored ensembling strategies to decrease a larger  $K$  to a much smaller value using post-processing techniques like clustering or non-maximum suppression. Nonetheless, these strategies often introduce additional computational burdens and latency. This finding and constraint motivate us to work on aggregation strategies to effectively pool out the best prediction in future.

#### 4.6.1. Discussion of limitations and future work

Our model does not utilize scene information, making it more challenging to achieve multimodal predictions that are all compliant with the scene. This is because the model solely relies on the motion dynamics of agents. We assume that all agents behave rationally,

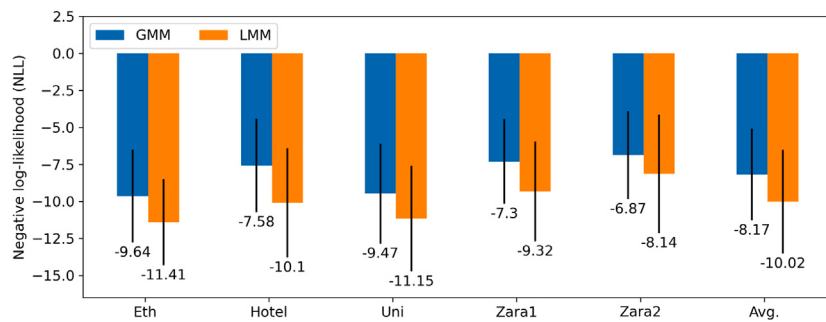


Fig. 9. The negative log-likelihood (NLL) between LMM and GMM tested on ETH/UCY. The error bars stand for the standard deviations.

Table 8

The ablation study of the self-attention (SA) mechanism and the GCN module on ETH/UCY.

SA	GCN	Eth	Hotel	Uni	Zara1	Zara2	Avg.
–	–	0.29/0.49	0.11/0.17	0.22/0.40	0.17/0.32	0.12/0.22	0.18/0.32
✓	–	0.29/0.45	0.10/0.15	0.21/0.40	0.17/0.32	0.12/0.22	0.18/0.31
✓	✓	0.26/0.42	0.10/0.15	0.21/0.38	0.16/0.28	0.12/0.21	0.17/0.29

Table 9

The comparison between the LSTM and MLP layers in the decoder on nuScenes.

Decoder layer	$ADE_5$	$FDE_5$	$ADE_{10}$	$FDE_{10}$
LSTM	2.00	4.46	1.57	3.28
MLP	2.03	4.51	1.58	3.28

Table 10

The comparison between the LSTM and MLP layers in the decoder on ETH/UCY.

Decoder layer	Eth	Hotel	Uni	Zara1	Zara2	Avg.
LSMT	0.26/0.42	0.10/0.15	0.21/0.38	0.16/0.28	0.12/0.21	0.17/0.29
MLP	0.27/0.43	0.11/0.16	0.21/0.39	0.17/0.31	0.12/0.22	0.18/0.30

Table 11

The comparison of different input features on nuScenes.

Position	Offset	$ADE_5$	$FDE_5$	$ADE_{10}$	$FDE_{10}$
✓	–	1.86	4.05	1.48	3.00
–	✓	1.87	4.08	1.46	2.97

Table 12

The comparison of different input features on ETH/UCY.

Position	Offset	Eth	Hotel	Uni	Zara1	Zara2	Avg.
✓	–	0.29/0.49	0.11/0.17	0.22/0.40	0.17/0.32	0.12/0.22	0.18/0.32
–	✓	0.26/0.42	0.10/0.15	0.21/0.38	0.16/0.28	0.12/0.21	0.17/0.29

Table 13

Performance difference between road user types and  $K$  modes.

Type	$ADE_5$	$FDE_5$	$ADE_{10}$	$FDE_{10}$
Bus	1.76	3.99	1.39	2.89
Car	1.85	4.02	1.48	3.02
Truck	1.85	3.93	1.50	2.91
Emergency vehicle	5.00	12.33	2.86	6.40
Construction vehicle	1.21	2.62	0.89	1.77
Average	1.85	4.02	1.48	3.00

such as following scene constraints, and that the observed trajectories include enough data samples that cover various areas within a given scene. However, without other explicit scene cues, there is a limitation in associating predictions with unseen areas, which can result in limited performance in achieving consistent predictions that align with the scene. Fig. 11 illustrates this issue, although some predicted trajectories closely match the ground truth trajectory, other predictions deviate from the lanes or violate scene constraints. GATraj's lack of scene

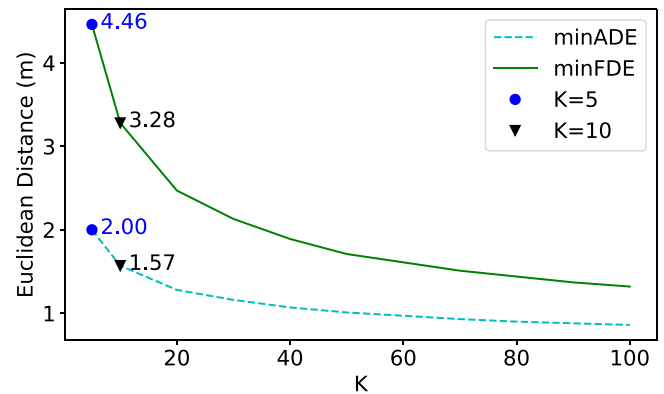


Fig. 10. The prediction results on nuScenes with increasing the number of components in the Laplacian MDN decoder. GATraj w/o GCN achieves 2.00/4.46 of  $ADE_5/FDE_5$  and 1.57/3.28 of  $ADE_{10}/FDE_{10}$ , respectively.

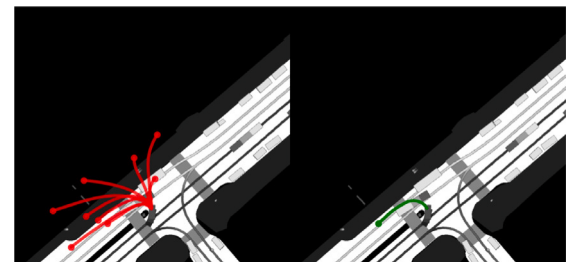


Fig. 11. An example of limited performance of GATraj when scene information is not considered. Left: predictions, right: the ground truth. The observed trajectory is denoted as dark rectangles with descending grayscales along the time steps – a darker color indicates an earlier time step. The prediction is in red dotted lines, and the corresponding ground truth is in green dotted lines. The HD map is only used for visualization and not used as extra contextual information for prediction. (For interpretation of the references to color in this figure legend, the reader is referred to the web version of this article.)

information is the main reason behind its inability to achieve scene-consistent predictions for vehicles driving on dedicated lanes in the nuScenes dataset.

Some recent models in trajectory prediction for autonomous driving, such as DenseTNT (Gu et al., 2021), HiVT (Zhou et al., 2022), and QCNet (Zhou et al., 2023b), have shown superior performance

on trajectory prediction for autonomous driving by exploiting HD maps with lane segment information. For these models to function optimally, it is necessary to have access to HD maps that are obtained in advance and are kept up-to-date. However, the acquisition and maintenance of high-quality and up-to-date HD maps is a costly and time-consuming endeavor. To address these limitations and enhance generalizability while reducing the burden of HD map annotation and acquisition, perception-based approaches using multiview camera images are gaining more and more attention. These approaches generate scene information on-the-fly and project it onto the ground plane from a bird's-eye view, facilitating the trajectory prediction task. Most recent examples of such approaches include BEVFormer by Li et al. (2022) and planning-based approaches by Hu et al. (2023). In future research, we will explore strategies to incorporate scene information, favorably through perception-based approaches, aiming to achieve scene-compliant multimodal predictions.

## 5. Conclusion

This paper proposes an attention-based graph model named GATraj for multi-agent trajectory prediction with a good balance of prediction accuracy and inference speed. We use attention mechanisms to learn spatial-temporal dynamics of agents like pedestrians and vehicles and a graph convolutional network to learn scene-centric interactions among them. A Laplacian mixture density network decoder predicts diverse and multimodal trajectories for each agent. GATraj achieves performance on par with the state-of-the-art models at a much higher prediction speed tested on the nuScenes benchmark for autonomous driving and state-of-the-art performance on the ETH/UCY benchmark for pedestrian trajectory prediction.

## Declaration of competing interest

The authors declare that they have no known competing financial interests or personal relationships that could have appeared to influence the work reported in this paper.

## Acknowledgments

This work is partially supported by the MSCA European Postdoctoral Fellowships under the 101062870 – VeVuSafety project and partially performed in the framework of project KaBa (Kamerabasierte Bewegungsanalyse aller Verkehrsteilnehmer für automatisiertes Fahren) supported by the European Regional Development Fund at VISCODA company.

## References

- Alahi, A., Goel, K., Ramanathan, V., Robicquet, A., Fei-Fei, L., Savarese, S., 2016. Social LSTM: Human trajectory prediction in crowded spaces. In: Proceedings of the IEEE/CVF Conference on Computer Vision and Pattern Recognition. pp. 961–971.
- Bae, I., Park, J.-H., Jeon, H.-G., 2022. Learning pedestrian group representations for multi-modal trajectory prediction. In: European Conference on Computer Vision. Springer, pp. 270–289.
- Caesar, H., Bankiti, V., Lang, A.H., Vora, S., Lioung, V.E., Xu, Q., Krishnan, A., Pan, Y., Baldan, G., Beijbom, O., 2020. nuScenes: A multimodal dataset for autonomous driving. In: Proceedings of the IEEE/CVF Conference on Computer Vision and Pattern Recognition. pp. 11621–11631.
- Chai, Y., Sapp, B., Bansal, M., Anguelov, D., 2020. MultiPath: Multiple probabilistic anchor trajectory hypotheses for behavior prediction. In: Kaelbling, L.P., Kragic, D., Sugiyama, K. (Eds.), Proceedings of the Conference on Robot Learning. In: Proceedings of Machine Learning Research, vol. 100, PMLR, pp. 86–99.
- Chang, M.-F., Lambert, J., Sangkloy, P., Singh, J., Bak, S., Hartnett, A., Wang, D., Carr, P., Lucey, S., Ramanan, D., et al., 2019. Argoverse: 3d tracking and forecasting with rich maps. In: Proceedings of the IEEE/CVF Conference on Computer Vision and Pattern Recognition. pp. 8748–8757.
- Chen, Y., Ivanovic, B., Pavone, M., 2022. ScePT: Scene-consistent, policy-based trajectory predictions for planning. In: Proceedings of the IEEE/CVF Conference on Computer Vision and Pattern Recognition. pp. 17103–17112.
- Cheng, H., Liao, W., Tang, X., Yang, M.Y., Sester, M., Rosenhahn, B., 2021a. Exploring dynamic context for multi-path trajectory prediction. In: IEEE International Conference on Robotics and Automation. IEEE, pp. 12795–12801.
- Cheng, H., Liao, W., Yang, M.Y., Rosenhahn, B., Sester, M., 2021b. AMENet: Attentive maps encoder network for trajectory prediction. ISPRS J. Photogramm. Remote Sens. 172, 253–266.
- Cho, K., Van Merriënboer, B., Bahdanau, D., Bengio, Y., 2014. On the properties of neural machine translation: Encoder-decoder approaches. In: Eighth Workshop on Syntax, Semantics and Structure in Statistical Translation (SSST-8).
- Cui, H., Radosavljevic, V., Chou, F.-C., Lin, T.-H., Nguyen, T., Huang, T.-K., Schneider, J., Djuric, N., 2019. Multimodal trajectory predictions for autonomous driving using deep convolutional networks. In: International Conference on Robotics and Automation. IEEE, pp. 2090–2096.
- Deo, N., Wolff, E., Beijbom, O., 2022. Multimodal trajectory prediction conditioned on lane-graph traversals. In: Proceedings of the Conference on Robot Learning. PMLR, pp. 203–212.
- Gao, J., Sun, C., Zhao, H., Shen, Y., Anguelov, D., Li, C., Schmid, C., 2020. Vectornet: Encoding hd maps and agent dynamics from vectorized representation. In: Proceedings of the IEEE/CVF Conference on Computer Vision and Pattern Recognition. pp. 11525–11533.
- Gilles, T., Sabatini, S., Tsishkou, D., Stanciulescu, B., Moutarde, F., 2022. Gohome: Graph-oriented heatmap output for future motion estimation. In: International Conference on Robotics and Automation. IEEE, pp. 9107–9114.
- Goodfellow, I., Pouget-Abadie, J., Mirza, M., Xu, B., Warde-Farley, D., Ozair, S., Courville, A., Bengio, Y., 2014. Generative adversarial nets. Adv. Neural Inf. Process. Syst. 27.
- Gu, T., Chen, G., Li, J., Lin, C., Rao, Y., Zhou, J., Lu, J., 2022. Stochastic trajectory prediction via motion indeterminacy diffusion. In: Proceedings of the IEEE/CVF Conference on Computer Vision and Pattern Recognition. pp. 17113–17122.
- Gu, J., Sun, C., Zhao, H., 2021. DenseTNT: End-to-end trajectory prediction from dense goal sets. In: Proceedings of the IEEE/CVF International Conference on Computer Vision. pp. 15303–15312.
- Gupta, A., Johnson, J., Fei-Fei, L., Savarese, S., Alahi, A., 2018. Social GAN: Socially acceptable trajectories with generative adversarial networks. In: Proceedings of the IEEE/CVF Conference on Computer Vision and Pattern Recognition. pp. 2255–2264.
- Helbing, D., Molnar, P., 1995. Social force model for pedestrian dynamics. Phys. Rev. E 51 (5), 4282.
- Ho, J., Jain, A., Abbeel, P., 2020. Denoising diffusion probabilistic models. Adv. Neural Inf. Process. Syst. 33, 6840–6851.
- Hochreiter, S., Schmidhuber, J., 1997. Long short-term memory. Neural Comput. 9 (8), 1735–1780.
- Hu, Y., Yang, J., Chen, L., Li, K., Sima, C., Zhu, X., Chai, S., Du, S., Lin, T., Wang, W., et al., 2023. Planning-oriented autonomous driving. In: Proceedings of the IEEE/CVF Conference on Computer Vision and Pattern Recognition. pp. 17853–17862.
- Hug, R., Becker, S., Hübner, W., Arens, M., 2021. Quantifying the complexity of standard benchmarking datasets for long-term human trajectory prediction. IEEE Access 9, 77693–77704.
- Johora, F.T., Yang, D., Müller, J.P., Özgürer, Ü., 2022. On the generalizability of motion models for road users in heterogeneous shared traffic spaces. IEEE Trans. Intell. Transp. Syst.
- Kalman, R.E., 1960. A new approach to linear filtering and prediction problems. Trans. ASME-J. Basic Eng. 82 (Series D), 35–45.
- Kim, K., Lee, D., Essa, I., 2011. Gaussian process regression flow for analysis of motion trajectories. In: Proceedings of the IEEE/CVF International Conference on Computer Vision. IEEE, pp. 1164–1171.
- Kingma, D.P., Ba, J., 2015. Adam: A method for stochastic optimization. In: International Conference on Learning Representations.
- Kingma, D.P., Mohamed, S., Jimenez Rezende, D., Welling, M., 2014. Semi-supervised learning with deep generative models. Adv. Neural Inf. Process. Syst. 27.
- Kingma, D.P., Welling, M., 2014. Auto-encoding variational bayes. In: International Conference on Learning Representations.
- Kitani, K.M., Ziebart, B.D., Bagnell, J.A., Hebert, M., 2012. Activity forecasting. In: European Conference on Computer Vision. Springer, pp. 201–214.
- Kosaraju, V., Sadeghian, A., Martín-Martín, R., Reid, I., Rezatofighi, H., Savarese, S., 2019. Social-bigat: Multimodal trajectory forecasting using bicycle-gan and graph attention networks. Adv. Neural Inf. Process. Syst. 32.
- Lee, N., Choi, W., Vernaza, P., Choy, C.B., Torr, P.H., Chandraker, M., 2017. Desire: Distant future prediction in dynamic scenes with interacting agents. In: Proceedings of the IEEE/CVF Conference on Computer Vision and Pattern Recognition. pp. 336–345.
- Lee, M., Sohn, S.S., Moon, S., Yoon, S., Kapadia, M., Pavlovic, V., 2022. MUSE-VAE: Multi-scale VAE for environment-aware long term trajectory prediction. In: Proceedings of the IEEE/CVF Conference on Computer Vision and Pattern Recognition. pp. 2221–2230.
- Lerner, A., Chrysanthou, Y., Lischinski, D., 2007. Crowds by example. In: Computer Graphics Forum, Vol. 26. Wiley Online Library, pp. 655–664.
- Li, Z., Wang, W., Li, H., Xie, E., Sima, C., Lu, T., Qiao, Y., Dai, J., 2022. BEVFormer: Learning bird's-eye-view representation from multi-camera images via spatiotemporal transformers. In: European Conference on Computer Vision. Springer, pp. 1–18.

- Liu, Y., Zhang, J., Fang, L., Jiang, Q., Zhou, B., 2021. Multimodal motion prediction with stacked transformers. In: Proceedings of the IEEE/CVF Conference on Computer Vision and Pattern Recognition. pp. 7577–7586.
- Ma, Y.J., Inala, J.P., Jayaraman, D., Bastani, O., 2021. Likelihood-based diverse sampling for trajectory forecasting. In: Proceedings of the IEEE/CVF International Conference on Computer Vision. pp. 13279–13288.
- Makansi, O., Ilg, E., Cicek, O., Brox, T., 2019. Overcoming limitations of mixture density networks: A sampling and fitting framework for multimodal future prediction. In: Proceedings of the IEEE/CVF Conference on Computer Vision and Pattern Recognition. pp. 7144–7153.
- Mao, W., Xu, C., Zhu, Q., Chen, S., Wang, Y., 2023. Leapfrog diffusion model for stochastic trajectory prediction. In: Proceedings of the IEEE/CVF Conference on Computer Vision and Pattern Recognition. pp. 5517–5526.
- Meng, M., Wu, Z., Chen, T., Cai, X., Zhou, X., Yang, F., Shen, D., 2022. Forecasting human trajectory from scene history. *Adv. Neural Inf. Process. Syst.* 35, 24920–24933.
- Nayakanti, N., Al-Rfou, R., Zhou, A., Goel, K., Refaat, K.S., Sapp, B., 2022. Wayformer: Motion forecasting via simple & efficient attention networks. arXiv preprint arXiv: 2207.05844.
- Ngiam, J., Vasudevan, V., Caine, B., Zhang, Z., Chiang, H.-T.L., Ling, J., Roelofs, R., Bewley, A., Liu, C., Venugopal, A., Weiss, D.J., Sapp, B., Chen, Z., Shlens, J., 2022. Scene Transformer: A unified architecture for predicting future trajectories of multiple agents. In: International Conference on Learning Representations.
- Pang, B., Zhao, T., Xie, X., Wu, Y.N., 2021. Trajectory prediction with latent belief energy-based model. In: Proceedings of the IEEE/CVF Conference on Computer Vision and Pattern Recognition. pp. 11814–11824.
- Park, D., Ryu, H., Yang, Y., Cho, J., Kim, J., Yoon, K.-J., 2023. Leveraging future relationship reasoning for vehicle trajectory prediction. In: International Conference on Learning Representations.
- Pellegrini, S., Ess, A., Schindler, K., Van Gool, L., 2009. You'll never walk alone: Modeling social behavior for multi-target tracking. In: Proceedings of the IEEE/CVF International Conference on Computer Vision. IEEE, pp. 261–268.
- Phan-Minh, T., Grigore, E.C., Boulton, F.A., Beijbom, O., Wolff, E.M., 2020. Covernet: Multimodal behavior prediction using trajectory sets. In: Proceedings of the IEEE/CVF Conference on Computer Vision and Pattern Recognition. pp. 14074–14083.
- Rezende, D., Mohamed, S., 2015. Variational inference with normalizing flows. In: International Conference on Machine Learning. PMLR, pp. 1530–1538.
- Rhinehart, N., McAllister, R., Kitani, K., Levine, S., 2019. Precog: Prediction conditioned on goals in visual multi-agent settings. In: Proceedings of the IEEE/CVF International Conference on Computer Vision. pp. 2821–2830.
- Richardson, E., Weiss, Y., 2018. On GANs and GMMs. *Adv. Neural Inf. Process. Syst.* 31.
- Rumelhart, D.E., Hinton, G.E., Williams, R.J., 1986. Learning representations by back-propagating errors. *Nature* 323 (6088), 533–536.
- Sadeghian, A., Kosaraju, V., Sadeghian, A., Hirose, N., Rezatofighi, H., Savarese, S., 2019. SoPhie: An attentive gan for predicting paths compliant to social and physical constraints. In: Proceedings of the IEEE/CVF Conference on Computer Vision and Pattern Recognition. pp. 1349–1358.
- Salzmann, T., Ivanovic, B., Chakravarty, P., Pavone, M., 2020a. Trajectron++. URL <https://github.com/StanfordASL/Trajectron-plus-plus/issues/53>.
- Salzmann, T., Ivanovic, B., Chakravarty, P., Pavone, M., 2020b. Trajectron++: Dynamically-feasible trajectory forecasting with heterogeneous data. In: European Conference on Computer Vision. Springer, pp. 683–700.
- Shi, X., Shao, X., Fan, Z., Jiang, R., Zhang, H., Guo, Z., Wu, G., Yuan, W., Shibasaki, R., 2020. Multimodal interaction-aware trajectory prediction in crowded space. In: Proceedings of the AAAI Conference on Artificial Intelligence. pp. 11982–11989.
- Shi, L., Wang, L., Long, C., Zhou, S., Tang, W., Zheng, N., Hua, G., 2023. Representing multimodal behaviors with mean location for pedestrian trajectory prediction. *IEEE Trans. Pattern Anal. Mach. Intell.*
- Shi, L., Wang, L., Long, C., Zhou, S., Zhou, M., Niu, Z., Hua, G., 2021. SGCN: Sparse graph convolution network for pedestrian trajectory prediction. In: Proceedings of the IEEE/CVF Conference on Computer Vision and Pattern Recognition. pp. 8994–9003.
- Sun, Q., Huang, X., Gu, J., Williams, B.C., Zhao, H., 2022. M2I: From factored marginal trajectory prediction to interactive prediction. In: Proceedings of the IEEE/CVF Conference on Computer Vision and Pattern Recognition. pp. 6543–6552.
- Sun, P., Kretschmar, H., Dotiwalla, X., Chouard, A., Patnaik, V., Tsui, P., Guo, J., Zhou, Y., Chai, Y., Caine, B., et al., 2020. Scalability in perception for autonomous driving: Waymo open dataset. In: Proceedings of the IEEE/CVF Conference on Computer Vision and Pattern Recognition. pp. 2446–2454.
- Sun, J., Li, Y., Fang, H.-S., Lu, C., 2021. Three steps to multimodal trajectory prediction: Modality clustering, classification and synthesis. In: Proceedings of the IEEE/CVF International Conference on Computer Vision. pp. 13250–13259.
- Varadarajan, B., Hefny, A., Srivastava, A., Refaat, K.S., Nayakanti, N., Cornman, A., Chen, K., Douillard, B., Lam, C.P., Anguelov, D., et al., 2022. Multipath++: Efficient information fusion and trajectory aggregation for behavior prediction. In: International Conference on Robotics and Automation. IEEE, pp. 7814–7821.
- Vaswani, A., Shazeer, N., Parmar, N., Uszkoreit, J., Jones, L., Gomez, A.N., Kaiser, L., Polosukhin, I., 2017. Attention is all you need. In: Advances in Neural Information Processing Systems. pp. 5998–6008.
- Wang, X., Su, T., Da, F., Yang, X., 2023. Prophnet: Efficient agent-centric motion forecasting with anchor-informed proposals. In: Proceedings of the IEEE/CVF Conference on Computer Vision and Pattern Recognition. pp. 21995–22003.
- Welling, M., Kipf, T.N., 2017. Semi-supervised classification with graph convolutional networks. In: International Conference on Learning Representations.
- Wilson, B., Qi, W., Agarwal, T., Lambert, J., Singh, J., Khandelwal, S., Pan, B., Kumar, R., Hartnett, A., Pontes, J.K., et al., 2021. Argoverse 2: Next generation datasets for self-driving perception and forecasting. In: Thirty-Fifth Conference on Neural Information Processing Systems: Datasets and Benchmarks Track (Round 2).
- Xu, C., Mao, W., Zhang, W., Chen, S., 2022. Remember intentions: retrospective-memory-based trajectory prediction. In: Proceedings of the IEEE/CVF Conference on Computer Vision and Pattern Recognition. pp. 6488–6497.
- Xu, Y., Ren, D., Li, M., Chen, Y., Fan, M., Xia, H., 2021. Tra2tra: Trajectory-to-trajectory prediction with a global social spatial-temporal attentive neural network. *IEEE Robotics and Automation Letters* 6 (2), 1574–1581.
- Xu, C., Tan, R.T., Tan, Y., Chen, S., Wang, Y.G., Wang, X., Wang, Y., 2023. Eqmotion: Equivariant multi-agent motion prediction with invariant interaction reasoning. In: Proceedings of the IEEE/CVF Conference on Computer Vision and Pattern Recognition. pp. 1410–1420.
- Xue, H., Huynh, D.Q., Reynolds, M., 2018. SS-LSTM: A hierarchical LSTM model for pedestrian trajectory prediction. In: IEEE/CVF Winter Conference on Applications of Computer Vision. pp. 1186–1194.
- Ye, C., Zhao, H., Ma, L., Jiang, H., Li, H., Wang, R., Chapman, M.A., Junior, J.M., Li, J., 2022. Robust lane extraction from MLS point clouds towards HD maps especially in curve road. *IEEE Trans. Intell. Transp. Syst.* 23 (2), 1505–1518.
- Yu, C., Ma, X., Ren, J., Zhao, H., Yi, S., 2020. Spatio-temporal graph transformer networks for pedestrian trajectory prediction. In: European Conference on Computer Vision. Springer, pp. 507–523.
- Yuan, Y., Kitani, K., 2020. Dlow: Diversifying latent flows for diverse human motion prediction. In: European Conference on Computer Vision. Springer, pp. 346–364.
- Yuan, Y., Weng, X., Ou, Y., Kitani, K.M., 2021a. AgentFormer. URL <https://github.com/Khrylx/AgentFormer/issues/5>.
- Yuan, Y., Weng, X., Ou, Y., Kitani, K.M., 2021b. AgentFormer: Agent-aware transformers for socio-temporal multi-agent forecasting. In: Proceedings of the IEEE/CVF International Conference on Computer Vision. pp. 9813–9823.
- Zhang, P., Ouyang, W., Zhang, P., Xue, J., Zheng, N., 2019. SR-LSTM: State refinement for LSTM towards pedestrian trajectory prediction. In: Proceedings of the IEEE/CVF Conference on Computer Vision and Pattern Recognition. pp. 12085–12094.
- Zhou, H., Ren, D., Yang, X., Fan, M., Huang, H., 2023a. CSR: cascade conditional variational auto encoder with socially-aware regression for pedestrian trajectory prediction. *Pattern Recognition* 133, 109030.
- Zhou, Z., Wang, J., Li, Y.-H., Huang, Y.-K., 2023b. Query-centric trajectory prediction. In: Proceedings of the IEEE/CVF Conference on Computer Vision and Pattern Recognition. pp. 17863–17873.
- Zhou, Z., Ye, L., Wang, J., Wu, K., Lu, K., 2022. HiVT: Hierarchical vector transformer for multi-agent motion prediction. In: Proceedings of the IEEE/CVF Conference on Computer Vision and Pattern Recognition. pp. 8823–8833.
- Zhu, Y., Ren, D., Xu, Y., Qian, D., Fan, M., Li, X., Xia, H., 2021. Simultaneous past and current social interaction-aware trajectory prediction for multiple intelligent agents in dynamic scenes. *ACM Transactions on Intelligent Systems and Technology (TIST)* 13 (1), 1–16.